Proceedings of the 5th WSEAS International Conference on Applications of Electrical Engineering, Prague, Czech Republic, March 12-14, 2006 (pp90-95)

Thermal Modeling of a High-Speed Solid-Rotor Induction Motor

JANNE NERG
Department of Electrical Engineering
Lappeenranta University of Technology
P.O. Box 20, 53851 Lappeenranta
FINLAND
http://www.ee.lut.fi/en

Abstract: - A thermal model based on the lumped parameters for a high-speed solid-rotor induction motor with a slitted rotor is presented. The motor geometry is divided into 14 parts where the thermal resistances as well as different loss components, i.e. electromagnetic, gas flow and friction losses are computed. The model takes into account the heat transfer both in axial and radial directions of the motor. The evaluation of different loss components is discussed in detail.

Key-Words: - High-speed induction motor, solid rotor, thermal modeling, loss calculation.

1 Introduction

In electrical machines, the design of heat transfer is of equal importance as the electromagnetic design of the machine, since the thermal rise of the machine eventually decides the output power of the machine. As a matter of fact, the command of heat and mass transfer in an electric machine is far more difficult and complicated than the conventional electromagnetic design of an electric machine.

The problem of temperature raise is twofold: first, in most motors, adequate heat removal is ensured with the thermal convection of air, thermal conduction through the fastening of the machine, and thermal radiation. In machines with high power density, also direct cooling methods can be applied. In these cases the cooling fluid flows through the machine removing heat from the interior parts of the machine. Second, in addition to the question of heat removal also the distribution of heat sources, i.e. losses, in different parts of the machine has to be considered. The distribution of the heat in the machine can be evaluated, when the distribution of the losses in different parts of the machine as well as the heat removal power are exactly known.

The traditional way to design the main dimensions of the electrical machine is to use the utilization factors reported e.g. in [1]. The method usually gives satisfactory results: the motor achieves the desired performance, and temperature limits are not exceeded. However, if the designer wants to improve the performance of the motor, reduce the dimensions, vary the construction, test new cooling methods or try cheaper materials then effective loss-calculation and thermal-analysis tools are required.

Many researchers have developed thermal-analysis methods for electrical machines. The most common approach is to utilize lumped parameters, i.e. thermal resistance networks, presented e.g. in [2]-[4]. In these models both radial and axial heat transfer inside the machine was taken into account and an accurate enough thermal analysis for everyday design purposes was achieved with only a fraction of computation effort. A totally FEM based combined magneto-thermal analysis is shown in [5], but it is more suitable to the applications where the main heat-transfer path inside the machine is in the radial direction. Furthermore, the computation time needed is much longer compared to the thermal network analysis.

In this paper a lumped parameter thermal model for a gas cooled, high-speed solid-rotor induction motor with axially slitted rotor is presented. The model utilizes T-equivalent circuits as elementary components to model different parts of the machine. Convection heat transfer and contact transitions are also modeled using thermal resistances. The gas flow and friction losses of the machine are evaluated using analytical equations. The electromagnetic losses of the machine are calculated using finite element method.

2 Description of the Thermal Model

The developed thermal model consists of a gas flow model of the cooling fluid and a thermal resistance model of the machine. The gas flow model is used to compute the mass flow rate of the cooling fluid needed at a given temperature rise of the cooling fluid as well as the fluid velocity and convection coefficients at different parts of the machine. In the thermal resistance model the motor geometry is divided into a number of lumped components, each

component having a heat source and interconnections to neighboring components through a linear mesh of thermal resistances. Each component is modeled in terms of a thermal node [6], approximating the mean temperature within the corresponding component. All the heat generation, i.e. losses, are introduced as a point source at this node.

A one half of the geometry of a high-speed solid rotor induction motor with a slitted solid rotor is shown in Fig. 1. The geometry is divided into 14 components. The lumped parameters of the motor are, in case of a conduction heat transfer, evaluated from the dimensional information of the machine and the thermal properties of the corresponding materials. The lumped parameters describing the convective heat transfer are evaluated from the geometry and convection coefficients obtained from the fluid flow model. However, the thermal contact resistances due to the contact transitions e.g. between the stator core and the frame are obtained from the experimental data presented in [3] - [4].

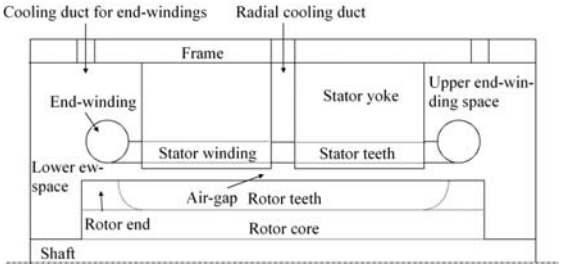

Fig. 1. The geometry of the high-speed solid rotor induction motor.

2.1 Conduction heat transfer

The thermal resistances describing the conduction heat transfer of all the components having a cylindrical form are obtained using the equations developed to a general cylindrical component, shown in Fig. 2. As it is described in [2], it is assumed that the heat flow in the radial and axial directions are independent, a single mean temperature describes the heat flow both in the radial and axial directions, no circumferential heat flow exists, and the heat generation is uniformly distributed inside the cylinder. As a solution of the heat conduction equations in both axial and radial directions, the separate three-terminal networks, shown in Fig. 3, are obtained. In each network, two of the terminals represent the appropriate surface temperatures of the component and the third terminal represents the mean temperature of the component. The two networks are connected in the mean temperature node. The losses of the component are injected there as well.

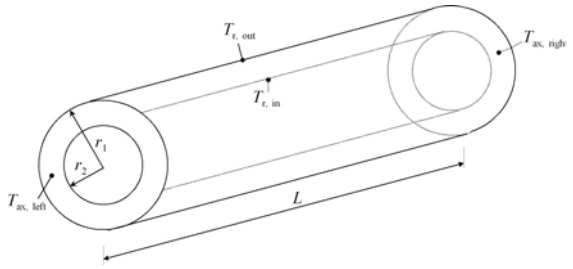

Fig. 2. General cylindrical component.

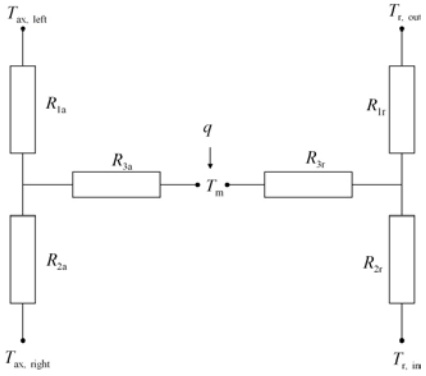

Fig. 3. Independent axial and radial thermal networks. T_m is the mean temperature node and q is the loss of the component.

The values of the thermal resistances in Fig. 3 are given in terms of the dimensions of the cylinder and the axial and radial thermal conductivities λ_{axial}, λ_{radial} of the material as

$$R_{1a} = R_{2a} = \frac{L}{2\pi\lambda_{axial}\left(r_1^2 - r_2^2\right)}, \tag{1}$$

$$R_{3a} = \frac{-L}{6\pi\lambda_{axial}\left(r_1^2 - r_2^2\right)}, \tag{2}$$

$$R_{1r} = \frac{1}{4\pi\lambda_{radial}L}\left[1 - \frac{2r_2^2 \ln\left(\frac{r_1}{r_2}\right)}{\left(r_1^2 - r_2^2\right)}\right], \tag{3}$$

$$R_{2r} = \frac{1}{4\pi\lambda_{radial}L}\left[\frac{2r_1^2 \ln\left(\frac{r_1}{r_2}\right)}{\left(r_1^2 - r_2^2\right)} - 1\right], \tag{4}$$

$$R_{3r} = \frac{-1}{8\pi\lambda_{radial}L}\left[r_1^2 + r_2^2 - \frac{4r_1^2 r_2^2 \ln\left(\frac{r_1}{r_2}\right)}{\left(r_1^2 - r_2^2\right)} \right]. \quad (5)$$

Due to the rotor slitting the rotor teeth are trapezoidal. The axial thermal network of the rotor teeth can be evaluated using the equations presented for the general cylindrical component.

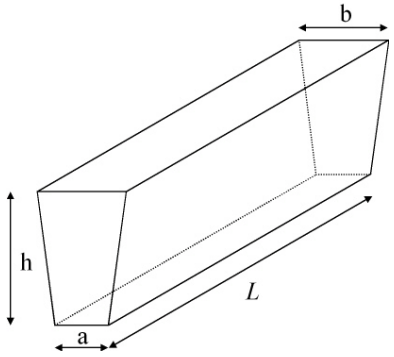

Fig. 4. The geometry of the rotor tooth.

The radial thermal network of the rotor teeth is obtained using the equations [7]

$$R_{1r} = \frac{h_{tooth}}{2\lambda_{radial}L(b-a)}\left[1 - \frac{2a^2 \ln\left(\frac{b}{a}\right)}{\left(b^2 - a^2\right)} \right], \quad (6)$$

$$R_{2r} = \frac{h_{tooth}}{2\lambda_{radial}L(b-a)}\left[\frac{2b^2 \ln\left(\frac{b}{a}\right)}{\left(b^2 - a^2\right)} - 1 \right], \quad (7)$$

$$R_{3r} \approx \frac{-\left(R_{1r} + R_{2r}\right)}{6}. \quad (8)$$

2.2 Convective heat transfer

The convection heat transfer between solid surfaces and cooling gas is modeled using a single thermal resistance $R_{convection}$ defined as

$$R_{convection} = \frac{1}{\alpha A}, \quad (9)$$

where α is the convection coefficient and A is the surface area. The thermal contact resistances due to the contact transitions are modeled in a similar manner by substituting the convection coefficient with the contact heat transfer coefficient.

The most important convection coefficients to be evaluated are the convection coefficients between the stator and the air-gap as well as between the rotating rotor and the air-gap. This is due to the fact that in these locations, the two main parts where the losses are generated are closest together. The convective heat transfer in the air-gap region of the high-speed electric machine is calculated using the following set of equations [8]

$$\mathrm{Nu} = 0.0214\left(\mathrm{Re}^{0.8} - 100\right)\mathrm{Pr}^{0.4}\left[1 + \left(\frac{d_h}{L}\right)^{0.66} \right], \quad (10)$$

$$\mathrm{Nu} = \frac{\alpha d_h}{\lambda}, \quad (11)$$

$$\mathrm{Re} = \frac{\rho v_{red} d_h}{\mu}, \quad (12)$$

$$d_h = \delta\sqrt{\frac{8}{3}}, \quad (13)$$

$$v_{red} = \sqrt{\left(\frac{\omega R}{2}\right)^2 + v_{axial}^2}, \quad (14)$$

where Nu is the Nusselt number, Re is the Reynolds number, Pr is the Prandl number, d_h is the hydraulic diameter, L is the axial length of the air-gap, δ is the radial length of the air-gap, ρ is the mass density of the cooling fluid, μ is the dynamic viscosity of the fluid, v_{red} is the reduced velocity in the helical direction in the air-gap, ω is the angular velocity of the rotor, R is the outer radius of the rotor and v_{axial} is the axial velocity of the cooling fluid.

3 Losses

The internal heat losses in electrical machines can be divided into electrical, friction and gas-flow losses. In this paper the losses due to the ventilators are not taken into account, because they do not act as an internal heat source but turn into heat in the ventilator thus heating the cooling fluid before it enters the electrical machine.

The friction and gas-flow losses are calculated using analytical methods, but the electromagnetic losses, i.e. iron losses in the stator and the rotor core as well as the Joule losses in the stator windings are

calculated using a two-dimensional finite element analysis. A FEM based electromagnetic analysis was chosen because the iron losses of the motor can be calculated more accurately than it would be the case using the analytical methods.

3.1 Friction losses

In high-speed machines the losses due to the gas friction are of significant importance. The rotating rotor gives a tangential velocity component for the air-gap gas. In addition, the gas has also an axial velocity component if the cooling gas is blown through the air-gap. Both the tangential and axial velocities affect the friction torque of the machine thus generating friction losses. The friction losses occur in the air-gap, rotor ends and shaft. A comprehensive analysis on the friction losses of high-speed machines is reported in [4].

The friction losses in the air-gap and rotor ends can be estimated by the equations derived for rotating cylinders in enclosures or in free space. The friction power P_{fr} associated with the resisting drag torque of a rotating cylinder can be written as [4]

$$P_{\mathrm{fr}} = k_1 C_{\mathrm{T}} \rho \pi \omega^3 r^4 l, \tag{15}$$

where C_{T} is the torque coefficient, ρ is the mass density of the fluid, ω is the angular velocity, r is the radius, l is the length of the cylinder and k_1 is the roughness coefficient the value of which is 1.0 for smooth surfaces and typically 2…4 for axially slotted surfaces. Because of the very complicated nature of the gas flow in a slotted rotor surface the torque coefficient must usually be determined by measurements.

When a cylinder is rotating in free space i.e. without the stator, one way to determine the nature of the tangential gas flow exerted by the rotating cylinder is to use the tip Reynolds number that determines the ratio of between the inertia and viscous forces

$$\mathrm{Re}_{\mathrm{r}} = \frac{\rho \omega r^2}{\mu}, \tag{16}$$

where μ is the dynamic viscosity of the fluid.

In order to take the effect of the enclosure, i.e. the stator, into account, the radial air-gap length has to be included in the Reynolds number. This is done in the Coquette Reynolds number, defined as

$$\mathrm{Re}_{\delta} = \frac{\rho u \delta}{\mu}, \tag{17}$$

where δ is the radial air-gap length and u is the peripheral speed of the rotor. According to the measurements reported in [9] the torque coefficients equations within the different flow regimes are

$$C_{\mathrm{T}} = 0.515 \frac{\left(\frac{\delta}{r}\right)^{0.3}}{\mathrm{Re}_{\delta}^{0.5}} \quad \left(500 < \mathrm{Re}_{\delta} < 10^4\right), \tag{18}$$

$$C_{\mathrm{T}} = 0.0325 \frac{\left(\frac{\delta}{r}\right)^{0.3}}{\mathrm{Re}_{\delta}^{0.2}} \left(10^4 < \mathrm{Re}_{\delta}\right). \tag{19}$$

Equations (18) and (19) have been tested with cylinders having relative air-gap lengths from 0.07 to 1, and the experimental data was within ±9 % the calculated curve. When the relative radial air-gap increases, at some point the tangential flow is not affected by the stationary outer cylinder any more, and the equations for free cylinders have to be used [4].

The friction losses increase if there is an axial gas flow through the air-gap. The rotor forces the cooling gas into a tangential movement and some power is needed for this acceleration. If the radial air-gap length is small compared to the rotor radius, the power loss can be approximated with

$$P_{\mathrm{fr,a}} = k_2 q_{\mathrm{m}} u^2, \tag{20}$$

where k_2 is the velocity factor and q_{m} is the mass flow rate of the cooling gas. The velocity factor depends on whether the flow is laminar or turbulent and the roughness of the air-gap surfaces. According to [10], the theoretical velocity factor gets a value of 0.48 in turbulent flow. However, the real value for the velocity factor can be expected to be much lower. According to the results reported in [11], the velocity factor, in case of a smooth rotor surface, gets a value of 0.18 for a smooth stator surface and 0.15 for a rough, i.e. slotted stator surface. Thereby, the stator slotting decreases the losses associated with the cooling gas flow through the air-gap. If the rotor surface is rough, the velocity factor can be expected to be close to the theoretical value of 0.48 [12].

The ends of the rotor do also have friction losses. The nature of the tangential flow is determined with

the tip Reynolds number. The power needed to rotate an end is

$$P_{\mathrm{fr,end}} = \frac{1}{2} C_{\mathrm{T}} \rho \omega^3 \left(r_2^5 - r_1^5 \right), \tag{21}$$

where r_2 and r_1 are the outer and inner radius of the end, respectively. In electrical machines the free space for the rotor ends in the end-winding area is typically large, and the rotor end acts like a centrifugal pump. When the rotor end is assumed to rotate in free space, the torque coefficient is [13]

$$C_{\mathrm{T}} = \frac{3.87}{\mathrm{Re}_{\mathrm{r}}^{0.5}} \quad \left(\mathrm{Re}_{\mathrm{r}} < 3 \cdot 10^5 \right), \tag{22}$$

$$C_{\mathrm{T}} = \frac{0.146}{\mathrm{Re}_{\mathrm{r}}^{0.5}} \quad \left(3 \cdot 10^5 < \mathrm{Re}_{\mathrm{r}} \right). \tag{23}$$

3.2 Electromagnetic losses

A two-dimensional, non-linear, time-stepping finite element method was utilized to the electromagnetic analysis of the high-speed solid-rotor induction motor. The electromagnetic field of the motor in the Cartesian plane can be described in terms of magnetic vector potential $\boldsymbol{A}$ as

$$\mu_0 \sigma \frac{\partial \boldsymbol{A}}{\partial t} + \nabla \times \left(\frac{1}{\mu_{\mathrm{r}}} \nabla \times \boldsymbol{A} \right) = \mu_0 \boldsymbol{J}, \tag{24}$$

where μ_0 is the magnetic permeability of free space, σ is electric conductivity, t is time, μ_{r} is relative magnetic permeability and $\boldsymbol{J}$ is current density. In order to model the power supply of the motor (24) was combined with the circuit equations.

The eddy-current losses $P_{\mathrm{eddy\text{-}current}}$ at each of the rotor regions, i.e. rotor teeth and rotor core are calculated by integrating the eddy-current loss density over the volume of the region using equation

$$P_{\mathrm{eddy\text{-}current}} = \int_{\mathrm{V}} \frac{|\boldsymbol{J}|^2}{\sigma}. \tag{25}$$

Iron losses of the stator core can be calculated by the loss separation method presented e.g. in [14]. According to the loss separation model the total iron loss is a sum of hysteresis, classical and excess losses. In FEM the iron loss density p_{iron} in the stator core is computed over one complete period using equation

$$\begin{aligned} \frac{1}{T} \int_0^T \mathrm{d}p_{\mathrm{iron}} \mathrm{d}t &= k_{\mathrm{h}} B_{\mathrm{m}}^2 f k_{\mathrm{f}} \\ &+ \frac{1}{T} \int_0^T \left[\sigma \frac{d^2}{12} \left(\frac{\mathrm{d}B}{\mathrm{d}t} \right)^2 + k_{\mathrm{e}} \left(\frac{\mathrm{d}B}{\mathrm{d}t} \right)^{3/2} \right] k_{\mathrm{f}} \mathrm{d}t \end{aligned} \tag{26}$$

where B_{m} is the maximum flux density at the node concerned, f is the frequency, d is the lamination sheet thickness, k_{h} is hysteresis loss coefficient, k_{e} is excess loss coefficient and k_{f} is stacking factor. The coefficients k_{h} and k_{e} can be calculated for studied electrical steel using the method presented in [15]. The total iron losses in the stator core are calculated by integrating iron loss density over the volume of the stator core. The hysteresis losses of the solid rotor volume can also be calculated using (26).

4 Computation of node temperatures

For steady-state analysis, the temperature rise of the each node of the thermal network relative to the reference temperature is calculated using the matrix equation

$$\boldsymbol{\Delta T} = \boldsymbol{G}^{-1} \boldsymbol{P}, \tag{27}$$

where $\boldsymbol{P}$ is the power loss vector containing the losses at each node and $\boldsymbol{\Delta T}$ is the temperature rise vector. In the developed thermal model the thermal resistances of different parts of the machine are used to generate a 14 × 14 thermal conductance matrix $\boldsymbol{G}$ defined as

$$\boldsymbol{G} = \begin{bmatrix} \sum_{i=1}^{14} \frac{1}{R_{1,i}} & -\frac{1}{R_{1,2}} & \cdots & -\frac{1}{R_{1,14}} \\ -\frac{1}{R_{2,1}} & \sum_{i=1}^{14} \frac{1}{R_{2,i}} & \cdots & -\frac{1}{R_{2,14}} \\ \vdots & \vdots & \ddots & \vdots \\ -\frac{1}{R_{14,1}} & -\frac{1}{R_{14,2}} & \cdots & \sum_{i=1}^{14} \frac{1}{R_{14,i}} \end{bmatrix}, \tag{28}$$

where the nth diagonal element is the sum of the network conductances connected to node n, and G(i, j) is the thermal conductance connecting the node-points i and j.

5 Application example

The developed thermal analysis model was tested in the thermal analysis of a 140 Hz, two-pole, three phase, 250 kW, solid rotor induction motor. The

number of the stator slots was 48 and the number of the rotor slits was 34. The geometry of the studied motor was shown earlier in Fig. 1. Because of the axial symmetry of the motor, only a half of the motor geometry was modeled in the thermal analysis. The motor is air cooled, i.e. the cooling air enters the radial cooling duct of the motor, flows through the air-gap and finally exits through the holes in end plates of the motor.

The temperatures at different parts of the motor were evaluated at the nominal point, i.e. the slip was 1.5 %. The inlet temperature of the cooling air was 20 °C. Calculated temperatures at the main locations of the machine are shown in Table 1.

Table 1.
Calculated temperatures of the test motor.

Motor location	Temperature (°C)
Stator yoke	87.0
Stator teeth	95.2
Stator winding	98.9
Stator end-winding	110.4
Rotor teeth	111.6
Rotor yoke	111.5

Calculated temperatures in the stator windings and in the stator end-windings were compared to the results obtained from the measurements. The measured values were 100 °C in the stator windings and 112 °C in the stator end-windings. The computed and measured temperatures correlate very well in these two locations.

6 Conclusions

A thermal model based on the lumped parameters for a high-speed solid-rotor induction motor with a slitted rotor was presented. The geometry was divided into 14 parts where the lumped parameters as well as different loss components were evaluated. The calculated results from the test motor showed good correlation with the values obtained from the measurements.

References:

[1] Vogt, K., *Berechnung electricher Maschinen*, VCH Verlagsgesellschaft mbH, Weinheim, 1996 (in german).

[2] Mellor, P. D., Roberts, D., Turner, D. R., "Lumped parameter thermal model for electrical machines of TEFC design", *IEE Proceedings-B*, Vol. 138, No. 5, pp. 205-218, September 1991.

[3] Kylander, G., *Thermal Modelling of Small Cage-Induction Motors,* Ph. D. thesis, Chalmers University of Technology, Gothenburg, Sweden, 1995.

[4] Saari, J., *Thermal analysis of high-speed induction machines*, Acta Polytechnica Scandinavia, Electrical Engineering Series no. 90, Diss. HUT, Espoo, Finland, 1998.

[5] Driesen, J., *Coupled Electromagnetic-Thermal Problems in Electrical Energy Transducers*, Ph. D. thesis, Katholieke Universiteit Leuven, Belgium, 2000.

[6] Perez, I. J., Kassakian, J. K., "A stationary thermal model for smooth air-gap rotating electrical machines", *Electrcl Machines and Electromechanics*, No. 3-4, pp. 285-303, 1979.

[7] Liu, Z. J., Howe, D., Mellor, P. D., "Thermal Analysis of Permanent Magnet Machines", In Proc. Sixth International Conference on Electrical Machines and Drives, pp. 359-364, 1993.

[8] VDI-Wärmeatlas, *Berechnungsblätter für den Wärmeübergang*, Fünfte erweiterte Aufgabe, VDI Verlag, Verlag des Vereins Deutscher Ingenieure, Düsseldorf, 1988.

[9] Bilgen, E., Boulos, R., Functional dependence of torque coefficient of coaxial cylinders on gap width and Reynolds numbers, Transactions of ASME, *Journal of Fluids Engineering,* series I, Vol. 95, 1973, pp. 122-126.

[10] Polkowski, J. W., Turbulent flow between coaxial cylinders with inner cylinder rotating, Transactions of ASME, *Journal of Engineering for Gas Turbines and Power*, Vol. 106, No. 1, 1984, pp. 128-135.

[11] Kreith, F., Convection heat transfer in rotating systems, Advances in Heat Transfer, Vol. 5, Academic Press Inc., 1968, pp. 129-246.

[12] Larjola, J. et al, Suurnopeustekniikan tutkimus LTKK:ssa, Loppuraportti, Tutkimusraportti, EN B-125, 1999 (in finnish).

[13] Huppunen, J., *High-speed solid-rotor induction machine – Electromagnetic calculation and design,* Acta Universitatis Lappeenrantaensis, no. 197, Diss, LUT, Lappeenranta, Finland, 2004.

[14] Bertotti, G., "General Properties of Power Losses in Soft Ferromagnetic Materials", *IEEE Trans. Magn.*, Vol. 24, No. 1, pp. 621-630, January 1988.

[15] Amar, M., Kaczmarek, R., "A General Formula for Prediction of Iron Losses Under Nonsinusoidal Voltage Waveform", *IEEE Trans. Magn.*, Vol. 31, No. 5, pp. 2504-2509, September 1995.